Since January 2020 Elsevier has created a COVID-19 resource centre with free information in English and Mandarin on the novel coronavirus COVID-19. The COVID-19 resource centre is hosted on Elsevier Connect, the company's public news and information website.

Bioorganic Chemistry 129 (2022) 106185

Contents lists available at ScienceDirect

Bioorganic Chemistry

journal homepage: www.elsevier.com/locate/bioorg

Acriflavine and proflavine hemisulfate as potential antivirals by targeting M^{pro}

Jing Liang [a,1], Mengzhu Zheng [c,1], Wei Xu [d,1], Yongkang Chen [d,1], Piyu Tang [a], Guoyi Wu [e,*], Peng Zou [e,*], Hua Li [a,b,c,*], Lixia Chen [a,*]

[a] Wuya College of Innovation, Key Laboratory of Structure-Based Drug Design & Discovery, Ministry of Education, Shenyang Pharmaceutical University, Shenyang 110016, China
[b] Institute of Structural Pharmacology & TCM Chemical Biology, College of Pharmacy, Fujian University of Traditional Chinese Medicine, Fuzhou 350122, China
[c] School of Pharmacy, Tongji Medical College, Huazhong University of Science and Technology, Wuhan 430030, China
[d] Key Laboratory of Medical Molecular Virology (MOE/NHC/CAMS), School of Basic Medical Sciences, Shanghai Institute of Infectious Disease and Biosecurity, Fudan University, Shanghai 200032, China
[e] Shanghai Public Health Clinical Center, Fudan University, Shanghai 201508, China

ARTICLE INFO

Keywords:
SARS-CoV-2
M^{pro} inhibitor
Acriflavine
Proflavine hemisulfate

ABSTRACT

The evolving SARS-CoV-2 epidemic buffets the world, and the concerted efforts are needed to explore effective drugs. M^{pro} is an intriguing antiviral target for interfering with viral RNA replication and transcription. In order to get potential anti-SARS-CoV-2 agents, we established an enzymatic assay using a fluorogenic substrate to screen the inhibitors of M^{pro}. Fortunately, Acriflavine (ACF) and Proflavine Hemisulfate (PRF) with the same acridine scaffold were picked out for their good inhibitory activity against M^{pro} with IC_{50} of 5.60 ± 0.29 μM and 2.07 ± 0.01 μM, respectively. Further evaluation of MST assay and enzymatic kinetics experiment *in vitro* showed that they had a certain affinity to SARS-CoV-2 M^{pro} and were both non-competitive inhibitors. In addition, they inhibited about 90 % HCoV-OC43 replication in BHK-21 cells at 1 μM. Both compounds showed nano-molar activities against SARS-CoV-2 virus, which were superior to GC376 for anti-HCoV-43, and equivalent to the standard molecule remdesivir. Our study demonstrated that ACF and PRF were inhibitors of M^{pro}, and ACF has been previously reported as a PL^{pro} inhibitor. Taken together, ACF and PRF might be dual-targeted inhibitors to provide protection against infections of coronaviruses.

1. Introduction

Severe acute respiratory syndrome coronavirus 2 (SARS-CoV-2) caused a pandemic sweeping the world and had become the focus of global health [1,2]. Although the marketing of inactivated vaccines, attenuated vaccines, and mRNA vaccines effectively blocked the SARS-CoV-2 pandemic and significantly reduced the incidence [3,4], the increased infectivity caused by the high-frequency gene mutation of SARS-CoV-2, especially the global spread of the Delta variant and Omicron variant, has bought another round of the storm [5,6]. It is urgent to develop anti-coronavirus drugs with multi-scale mechanisms.

As a cysteine protease, M^{pro} (main protease, also named 3C-like protease, $3CL^{pro}$) regulates viral RNA replication and transcription, has relatively conservative evolution in pathogenic β-coronavirus, and shares significant similarity in the catalytic dyad, His41 and Cys145. The active form of M^{pro} is a homodimer structure, and its *N*-finger residues authentic integrity is crucial for proteases activity. Besides, there is a lack of homologous protease in humans, which promotes it as one of the ideal targets for developing anti-coronavirus drugs [7–10].

Large numbers of M^{pro} inhibitors have been reported with a variety of screening methods, including virtual screening, FRET technology, cell model screening, and so on [11,12]. Among these, the in-silico techniques are currently the most widely used and convenient strategy. Typically, scientists used candidate targets to extensively screen the FDA-approved drug databases, natural product databases, clinical trial library, and previously reported coronavirus inhibitors, combined with

* Corresponding authors at: Wuya College of Innovation, Key Laboratory of Structure-Based Drug Design & Discovery, Ministry of Education, Shenyang Pharmaceutical University, Shenyang 110016, China (H. Li and L. Chen).
E-mail addresses: wuguoyi@163.com (G. Wu), zoupeng@shphc.org.cn (P. Zou), li_hua@hust.edu.cn (H. Li), syzyclx@163.com (L. Chen).
[1] These authors contributed equally to this work.

https://doi.org/10.1016/j.bioorg.2022.106185
Received 18 August 2022; Received in revised form 18 September 2022; Accepted 26 September 2022
Available online 7 October 2022

the molecular dynamics and pharmacological validation to explore their pharmacodynamics and potential binding mechanisms, which can be determined to identify the potential inhibitors or drug repurposing of M^{pro}[13–15]. At this stage, a variety of SARS-CoV-2 inhibitors have been found by this strategy, such as Ebselen [16], Baicalein [17,18], Plumbagin [19], Ginkgolic acid [20,21], Theaflavin 3-gallate [22], Theasinensin-D, Oolonghomobisflavan-A [23], DSPD-2/5/6 [24]. However, these inhibitors need to be further validated and researched to obtain candidacy for clinical trials.

In the present study, we performed an enzymatic assay using a fluorogenic substrate to screen the inhibitors of M^{pro}. Acriflavine (ACF) and Proflavine hemisulfate (PRF) were identified as micromolar-range inhibitors. On this basis, MST assay, enzyme activity experiment *in vitro*, molecular docking, and antiviral activity assay were conducted in-depth research. In summary, this study comprehensively elaborated that the ACF and PRF can be developed as good candidates for anti-coronaviral drugs *in vitro* and provided useful guidance for its drug repurposing in SARS-CoV-2 therapy.

2. Material and methods

The cDNA of SARS-CoV-2 M^{pro} (GenBank:MN908947.3) was cloned into pGEX-6P-1 vector (GE Healthcare, Cat.No:27-4597-01, USA). SARS-CoV-2 M^{pro} gene was constructed by Tsingke Biotechnology Company, China. Human rhinovirus (HRV) 3C protease was obtained from Prof. Li Yan, Huazhong University of Science and Technology. The fluorogenic substrate and compounds were purchased from meilunbio®, China. The ligand library contained 2817 compounds from ZINC database (https://zinc.docking.org/), as well as 1066 compounds separated from traditional Chinese herbals.

2.1. Expression and purification of M^{pro}

To obtain authentic SARS-CoV-2 M^{pro}, four amino acids (AVLQ) were added between the GST-tag and *N*-foreign DNA fragment and eight amino acids (GPHHHHHH) were added to the C-terminus when we constructed the plasmid. The plasmid was then transformed into TSINGKE TSC-E03 TSR2566 Chemically Competent Cells for protein expression.

The signal clone was pre-cultured at 37 °C in 100 ml Luria Broth (LB) medium with ampicillin (100 mg/mL) overnight, and then transferred into 4 L LB medium with ampicillin (100 mg/L). 4 mM isopropyl-d-thiogalactoside (IPTG) was adding until the A_{600} value to 0.8. After 16 h incubated at 18 ℃, the cells were harvested, resuspended in lysis buffer (20 mM Tris-HCl, pH 8.0, 150 mM NaCl, 1 % Triton-X100, 2 mM DTT), and lysed by Continuous High Pressure Cell Disrupter with 1000 bar at a time for 5 rounds on ice. Then cell debris was removed by centrifugation at 20,000 rpm, 4 °C for 30 min. The supernatants were loaded onto a Ni-NTA (GE Healthcare) affinity column and washed with buffer A1 (20 mM Tris-HCl, pH 7.5, 150 mM NaCl, 10 mM imidazole) and buffer A2 (20 mM Tris-HCl, pH 7.5, 150 mM NaCl, 20 mM imidazole) for five column volumes, respectively. 0.4 mg/mL HRV-3C protease was then added to samples of buffer A2 for cleaving the C-terminal eight amino acids at 4 C overnight. The resulting protein was loaded onto a Ni-NTA column to separate the His-tag-label protein or non-His-tag-label protein by buffer A1. The resulting protein sample was further purified to Superdex 75 10/300GL loaded by AKTA-pure (GE Healthcare). The purity of the recombinant protein was collected and confirmed by 15 % SDS-PAGE (Supplementary Information, S1). The pro-prepared protein with 2 mM DTT was stored at −80 ℃ for enzymatic inhibition assay and MST assay.

2.2. Enzymatic inhibition assay

An enzymatic assay using a fluorogenic substrate was applied to measure the inhibitory activity of compounds on M^{pro}. Firstly, the correctness of the enzyme activity system in this experiment was determined by assaying the effects of two reported positive drugs GC376 [25] and carmofur [9]. Secondly, a large-scale preliminary screening was launched, and the inhibition activities of candidate compounds were finally confirmed.

The compounds were dissolved in DMSO (20 μM final concentration), mixed with the reaction system (150 nM SARS-CoV-M^{pro}, 50 mM Tris-HCl, pH 7.3, 1 mM EDTA) and then incubated at 30 °C for 15 min. The reaction was initiated by adding fluorogenic substrate (MCA-AVLQSGFR(Dnp)-Lys-NH2) at a final concentration of 22 μM in 96-well black non-detachable plate. After that, the fluorescence signal at 320 nm (excitation)/405 nm (emission) were monitored every 2 s for 15 min by BioTEK Synergy H1 fluorescence spectrophotometer. The equivalent M^{pro}, fluorogenic substrate DMSO and positive control GC376 and carmofur were assayed as control simultaneous.

When the inhibition activity of compounds is up to 50 %, the complexes were picked out to determine the half-maximal inhibitory (IC_{50}) again. In detail, the complexes were assayed at ten different concentration between 0 and 40 μM, and the concentration of the enzyme was 150 nM. To further determine the inhibition mode by enzymatic kinetics study, the complexes were assayed at six different concentrations between 0 and 20 μM, and concentrations of enzyme was 150 nM, the substrates were assayed at eight different concentration between 0.78125 and 200 μM, respectively. The hydrolysis of the substrate was monitored again, and the rate of hydrolysis was determined in the linear range.

For each compound experiment was performed in triplicate. The IC_{50} values were calculated by plotting the average percentage inhibition against inhibitor concentration and fitting the data in GraphPad Prism 7.

2.3. Microscale thermophoresis (MST) assay

The pro-protein was diluted with buffer B (20 mM HEPES, pH 7.3, 1 mM EDTA) and kept constant at 10 μM. The tested compounds were diluted in proper concentration for the test. After incubating 100 μL pro-protein and isometric fluorochrome at room temperature lucifugally for 30 min, then loaded into Monolith™ (Germany) standard-treated capillaries to collect samples with a Norm. The fluorescence value was 2000–2500 AU. After that, the same amount of compounds and labeled samples were measured at 25 °C after 15 min incubation, while laser power was set to 20 % or 40 % using 30 *sec* on-time, and the LED power was set to 100 %. All experiments were repeated three times for each measurement. The dissociation constant K_d values were fitted by using the NT analysis.

2.4. Structure-based molecular docking

PDB ID: 6YB7/6LU7 in RCSB Protein Data Bank (https://www.pdb.org) is the best-resolution form of ligand-free and ligand-induced monomers in SARS-CoV-2 M^{pro}. Before docking, protein structures were optimized using Protein Preparation Wizard (Schrodinger), polar hydrogens and Gasteriger charges were added using AutodockTools (Vision-1.5.7).

The skeleton was acquired from PubChem (Compound CID: 7099, https://pubchem.ncbi.nlm.nih.gov). All torsions were chosen and Gasteriger charges were added using AutodockTools (Vision-1.5.7).

The active sites were defined according to the literature [26]. The first is target the “cryptic site” (CS): Lys5, Met6, Pro108, Gly109, Arg131, Trp218, Phe219, Tyr239, Glu240, Leu271, Leu272, Leu287, Glu288, Asp289, Glu290, Arg298, Gln299 and Val303. The second is target the “dimerization site” (DS): Arg4, Met6, Ser10, Gly11, Glu14, Asn28, Ser139, Phe140, Ser147, Glu166, Glu290 and Arg298. The third is the “ligand-induced substrate binding site” (ISBS): His41, Met49, Tyr54, Gly143, Ser144, Cys145, Phe140, Leu141, Asn142, His163, Met165, Glu166, Leu167, Pro168, His172, Phe185, Asp187, Gln189, Thr190, Ala191, Gln192.

In the case of CS and DS, 6YB7 was the chosen receptor, while in the case of ISBS, the 6LU7 was chosen. The grid-line of points in X-Y-Z dimension is 126-126-84 with 0.336 spacing at the center of X: 11.522, Y: 7.344, Z: −4.732 for CS. While the grid-line of points in the X-Y-Z dimension is 66-88-102 with 0.386 spacing at the center of X: 3.639, Y: −0.005, and Z: 4.985 for DS. Moreover, the grid-line of points in the X-Y-Z dimension is 56-56-70 with 0.464 spacing at the center of X: −15.106, Y: 12.610, and Z: 68.479 for ISBS. The docking calculation was performed in AutoDock Vina (Version-1.1.2), 2D ligand–protein interaction diagrams were generated by PoseView in Proteins Plus (https://proteins.plus/), and the 3D interaction diagrams were predicted in Pymol.

2.5. HCoV-OC43 and SARS-CoV-2 antiviral assay

The HCoV-OC43 antiviral assay was performed routinely by plaque assay as previously described with slight modification [27,28]. Briefly, BHK-21 cells were seeded in 6-well plates and cultured overnight. Then cells were infected with 100 plaque-forming units (PFU) HCoV-OC43 in the presence of compounds with different concentrations. After incubation at 33 °C for 2 h, the supernatant was removed and cells were supplemented with DMEM containing different concentrations of the compounds, 1.2 % Avicel (FMC Biopolymer, USA) and 2 % FBS. After 3 to 4 days post infection, BHK-21 cells were fixed and stained with 4 % formaldehyde containing 1 % crystal violet, and the number of plaques was counted after rinsing with water.

For testing the anti-SARS-CoV-2 efficacy of acriflavine and proflavine hemisulfate, plaque assay was conducted in a Biosafety Level 3 (BSL-3) laboratory of Fudan University as previously described [29]. Vero-E6 cells were first seeded into a 96-well plate. After cultured overnight, these two compounds were serially diluted in DMEM medium and incubated with authentic SARS-CoV-2 viruses for 30 min. The mixture was subsequently applied to the Vero-E6 cells and further incubated for 2 h. Subsequently, 1 % methyl cellulose (Sigma, USA) was added followed by culture for further 72 h. Finally, PBS containing 4 % paraformaldehyde and 1 % crystal violet was added for fixation and staining, and then plaques were counted after rinsing with water.

3. Results

3.1. Screening of SARS-CoV-2 M^{pro} inhibitors

The enzymatic activity was measured by time-dependent kinetics using a fluorogenic substrate MCA-AVLQSGFR(Dnp)-Lys-NH2 to identify the potential inhibitors of SARS-CoV-2 M^{pro}. The relative fluorescence unit (RFU) was used to measure the amount of substrate depletion. Based on that, the activity of M^{pro} could be tested through the measurement of K_m and V_{max} values. The specific experimental protocol has been reported in detail [9]. We first determined the previously reported potent inhibitors of M^{pro}, GC376, and carmofur. The dose–response curve was shown in Fig. 1**A and B**, the IC_{50} values of GC376 and carmofur were 0.12 μM and 0.67 μM, respectively. 2817 FDA-approved drugs and several natural products were first screened as the protocol described above. To our surprise, ACF and PRF showed an encouraging inhibitory effect with IC_{50} values of 5.60 μM and 2.07 μM (Fig. 1**C, D**), respectively. In brief, the results of the enzymatic assay implied that ACF and PRF would be developed as anti-SARS-CoV-2 reagents (Fig. 1).

3.2. Inhibition mode assays supported by enzymatic kinetic and MST

To further validate the inhibition mode of the ACF and PRF with M^{pro}, the enzyme kinetic parameters were determined. After the enzymatic reaction proceeded for about 15 min, it can be observed that a large amount of substrate was consumed. As shown in Fig. 2, it was observed that their inhibition activities had a good correlation with the concentration. The point we would like to raise was ACF with the constant K_m and concentration-dependent-decreased V_{max}, implying that ACF non-competitively inhibited M^{pro}. Similarly, in the study of inhibition mode measurement of PRF, K_m basically remained unchanged with the increase of compound concentration, while V_{max} decreased, indicating that PRF also non-competitively inhibited M^{pro} (Table 1).

Furthermore, MST assay had been used to identify the binding affinity between compounds and M^{pro}. ACF and PRF demonstrated that the K_d values were 86.60 ± 13.14 μM and 62.70 ± 9.54 μM, respectively

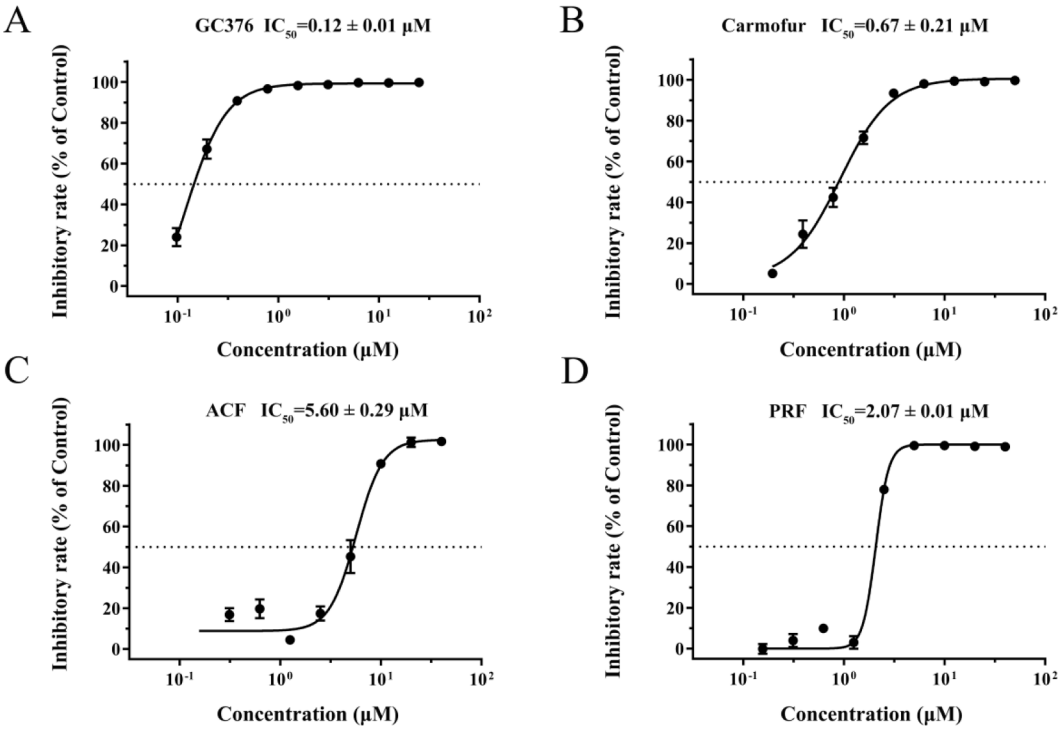

Fig. 1. Inhibition of the enzymatic activity of SARS-CoV-2 M^{pro} by enzymatic assay. A, GC376 against SARS-CoV-2 M^{pro}. B, Carmofur against SARS-CoV-2 M^{pro}. C, Representative curve for ACF against SARS-CoV-2 M^{pro}. D, Representative curve for PRF against SARS-CoV-2 M^{pro}. All data are shown as mean ± SD, n = 3.

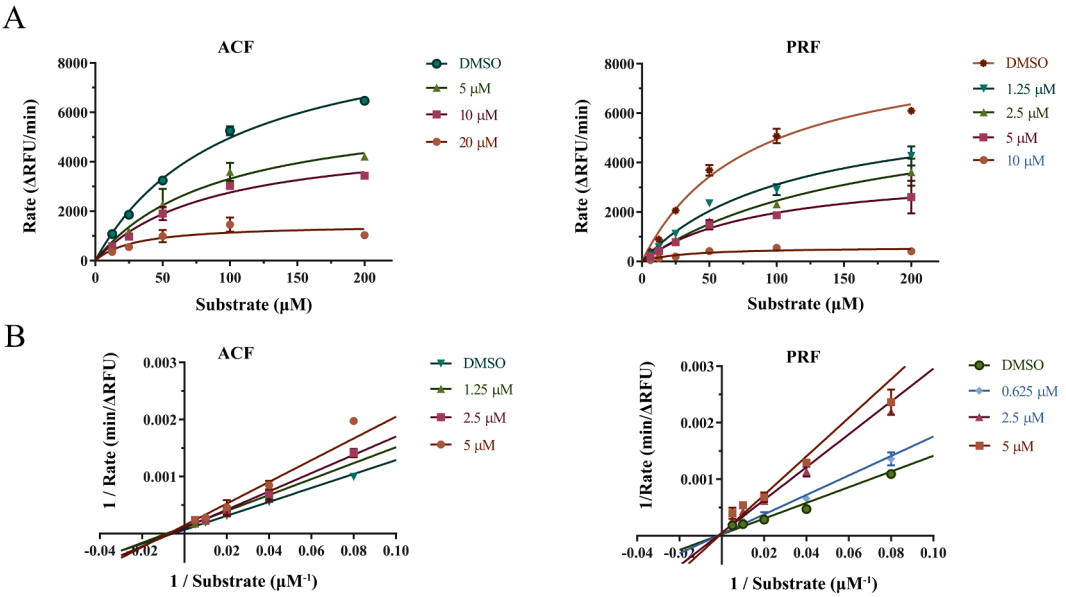

Fig. 2. Inhibition mode of ACF and PRF. A, Reaction rate of the fluorogenic substrate MCA-AVLQSGFR(Dnp)-Lys-NH2 catalyzed by SARS-CoV-2 M^{pro} in the presence of different concentration compounds. B, Enzyme kinetics curve by Lineweaver-Burk. All data are shown as mean ± SD, n = 3.

Table 1
The maximum reaction velocity (V_{max}) and constant (K_m) during the process of the Enzymatic-inhibitions reaction.

Compound (μM)	Kinetic parameter	0	1.25	2.5	5
ACF	Vmax (ΔRFU/min)	9877	9273	6245	6397
	Km (μM)	99.01	115.80	70.60	93.44
Compound (μM)	Kinetic parameter	0	0.625	2.5	5
PRF	Vmax (ΔfRFU/min)	8897	8888	6491	3740
	Km (μM)	79.74	113.00	164.10	89.94

(Fig. 3). The K_d was used to describe the binding affinity: the smaller K_d, the higher the affinity of the inhibitor to a target, the firmer the complexes. The encouraging K_d provided the groundwork for the potent inhibition. More than this, it was highly likely that the inhibition mode could be associated with the K_d. ACF and PRF were both non-competitive inhibitors, they had an affinity with the free M^{pro} and enzyme-substrate (ES) complexes. There was less interference of substrate with its binding to the target, therefore ACF and PRF had strong affinity with M^{pro} *in vitro*.

3.3. Molecular docking

Non-competitive inhibitors would bind to enzyme in sites rather than substrate binding sites (SBS). To better understand the binding mechanism between the compound and protein, we presumed its binding sites would deviate from the active pocket.

The present study revealed that there are three candidate-binding sites for inhibiting the M^{pro}. The first strategy is target the "cryptic site" (CS), which is a candidate allosteric site. The second strategy is target the "dimerization site" (DS), which could interrupt the dimeric conformation and inactive M^{pro}. The third is bound to the complex with the present of the substrate, named "ligand-induced substrate binding site" (ISBS). Thus, three plausible docking strategies were adopted and results were given as Fig. 4.

To our surprise, ACF was fitted well in three models, which presented the energy to CS (−6.079 kcal/mol), DS (−5.686 kcal/mol), and ISBS (−5.121 kcal/mol). For CS, the amino-terminal formed two hydrogen bonds with Gln110, and Glu240. Benzene contacted imidazole on His246 via pi-pi interaction. For DS, ACF was fitted well between the junctions of protomer, while it bound to Ser123 with one hydrogen, showing disrupted the interplay of dimerization stability. For ISBS, the amino-terminal formed hydrogen bonds with Ser46 and the inhibitor N3. Remarkably, the 10-N of ACF were involved the hydrogen with Gln189. Gln189 is utilized as one of the key residue of M^{pro} for

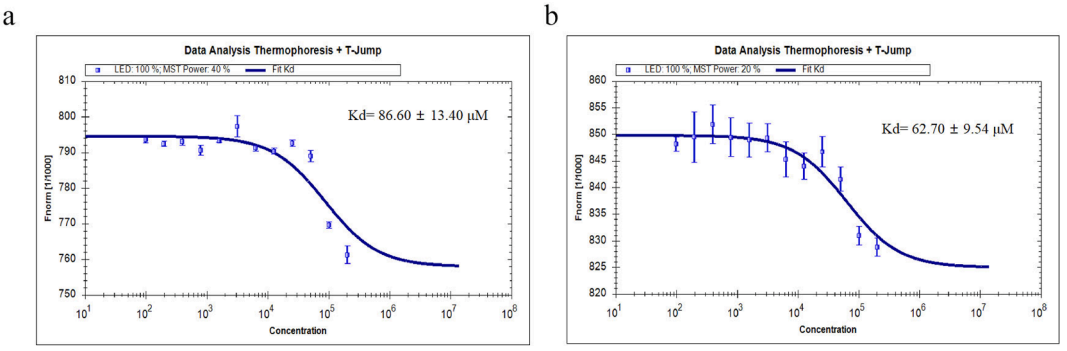

Fig. 3. The binding affinity between compounds and of SARS-CoV-2 M^{pro} measured with MST assay. A, ACF. B, PRF. The error bars represent the SD of each data point calculated from three independent thermophoresis measurements, $n = 3$.

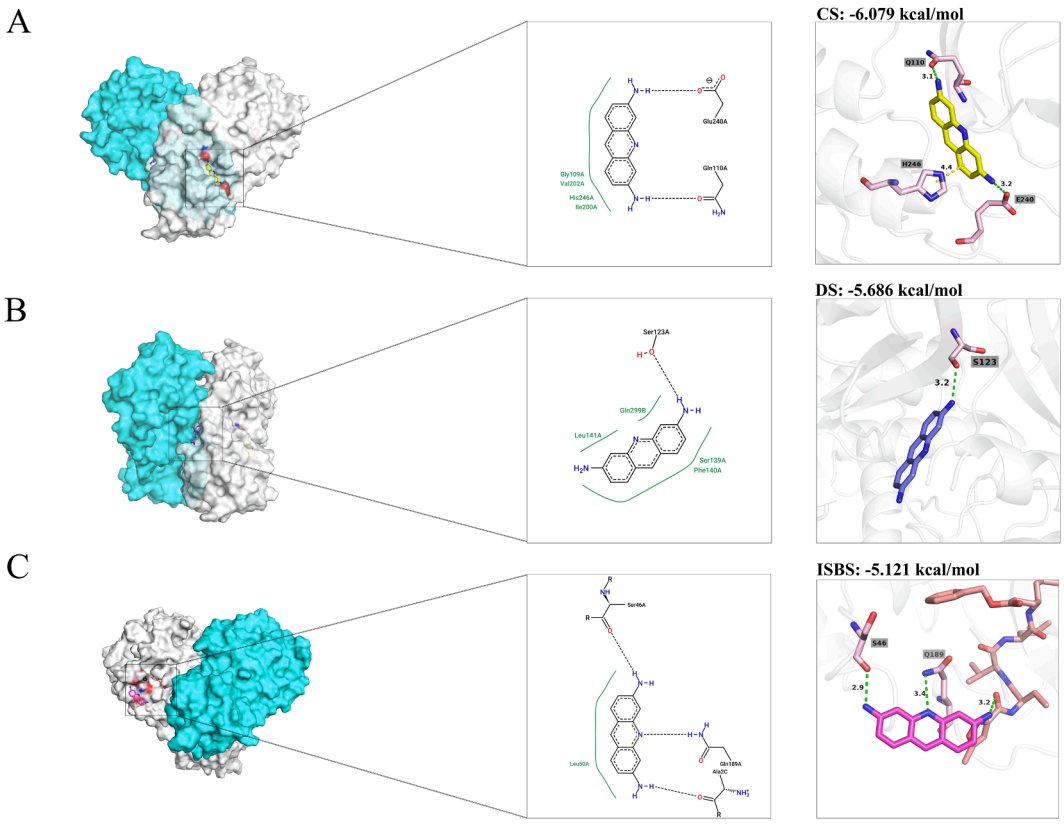

Fig. 4. Interaction analysis of Proflavine (ACF) with SARS-CoV-2 M^{pro} proteasea. A, The enlarged view of the "cryptic site" (CS). B, The enlarged view of "dimerization site" (DS). C, The enlarged view of the "ligand-induced substrate binding site" (ISBS). Note: Left panel: The overview of ACF in different sites. PDB ID: 6YB7 is shown in surface with two protomer, while protomer A is in cyans, protomer B is in gray. Middle panel: Two dimensions (2D) ACF-M^{pro} interaction diagram. Binding interactions of ACF to M^{pro} as analyzed by Proteins Plus. Right panel: The 3D visualization of interaction diagram. Both ligands and interacting residues are shown as sticks, while protein is depicted as cartoon. Hydrogen bonds are represented by the green-dashed line and pi-pi interaction are shown in yellow-dashed line. (For interpretation of the references to colour in this figure legend, the reader is referred to the web version of this article.)

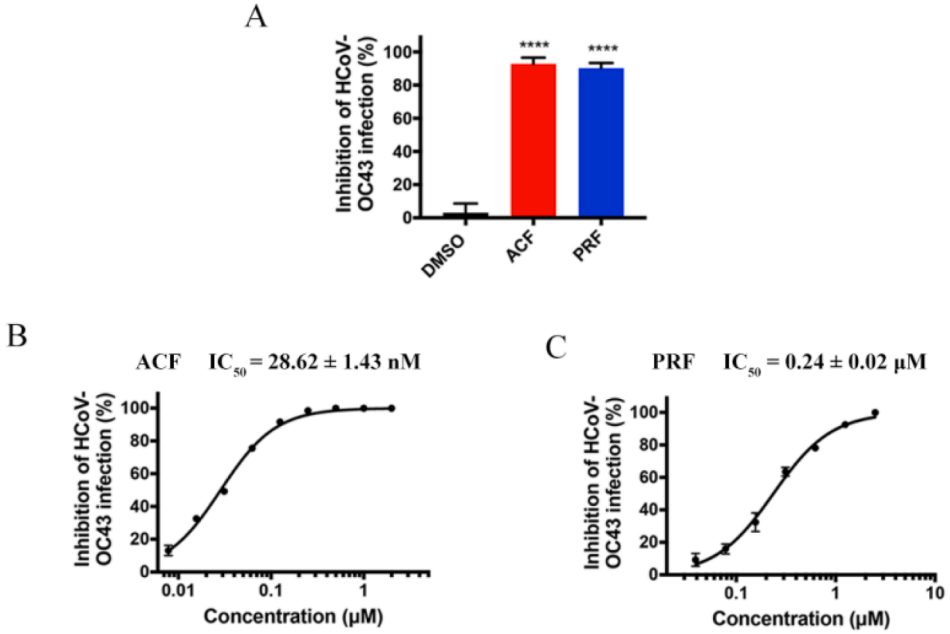

Fig. 5. Antiviral activities of the drug leads against HCoV-OC43. A, Antiviral activities of ACF and PRF against HCoV-OC43 at 1 μM. B, Dose–response curves for ACF against HCoV-OC43. C, Dose–response curves for PRF against HCoV-OC43. All data are shown as mean ± SD, n = 3. Probability (p) values were calculated by the unpaired two-tailed Student's-t-test between the compound and DMSO (**** $p < 0.0001$).

influencing the connecting loop between Domain II and III [30,31]. Darunavir, ritonavir, and saquinavir *etc*. had the comparable interactions with Gln189 [32], which implied that our compound had a broad possibility to bind to ISBS. Different docking strategies provided conformational variation in different sites. Taken together, these results indicated that there were diverse interaction patterns of acridine skeleton recognition by SARS-CoV-2 M^{pro}.

3.4. Antiviral assay

It's imperative to evaluate the antiviral activity of ACF and PRF against human β-coronavirus. One of the classical human β-coronaviruses, HCoV-OC43, was first used to evaluate the antiviral activity by plaque assay. HCoV-OC43 can replicate efficiently in BHK-21 cell, which was used as a host for virus [27,28,33]. Particularly, at a concentration of 1 μM, the inhibitory rate of ACF and PRF on OC43 reached about 90 %. Especially, ACF and PRF showed inhibition of HCoV-OC43 replication, with an IC_{50} value of 28.62 ± 1.43 nM and 0.24 ± 0.02 μM, respectively (Fig. 5), which were stated to be more effective than the positive control, GC376 (36.95 ± 2.92 nM).

Authentic SARS-CoV-2 was also used to evaluate the antiviral activity of ACF and PRF. In the experiment, the IC_{50} values of ACF and PRF against SARS-CoV-2 were 0.15 ± 0.02 μM and 0.13 ± 0.01 μM, respectively (Fig. 6), which showed the equivalent with the standard molecule remdesivir (0.19 ± 0.05 μM). The result was encouraging since nanomole-level antiviral activities opened a solid avenue for anti-SARS-CoV-2.

4. Discussion

The COVID-19 epidemic caused by SARS-CoV-2 infection has always been highly infectious since its outbreak [34]. The emergence of SARS-CoV-2 variants further enhances its infectivity and pathogenicity and reduces the protection of vaccines [10]. Hence, it is of great significance to develop anti-coronavirus drugs. The evolutionarily conserved M^{pro} plays an important role in regulating the RNA replication and transcription of the virus, and there is no protease similar to M^{pro} in the human body. Therefore, M^{pro} is a promising therapeutic target for the development of anti-coronavirus drugs.

A variety of screening methods have been reported for the screening and discovery of small molecule inhibitors of M^{pro}, including virtual screening [35], FRET technology [36–39], cell model screening[31], and phenotypic screening [40], *etc*. We constructed a nine-peptide-fluorogenic molecular as the substrate of M^{pro}, which recognize the sequence of -AVLQ/SGFRK- (the cleavage site is indicated by /) [41]. The value of RFU is applied to characterizing the activity of candidate compounds. Of note, since the fluorescent molecules are easily quenched, they need to be freshly prepared. In addition, some natural products may have fluorescent properties and can cause interference in the RFU value detection of the FRET screening. It is necessary to use the physical and chemical information of the database in time to eliminate the interference of these compounds effectively to improve the screening efficiency. Furthermore, considering that the enzyme kinetic reaction of M^{pro} is easily affected by environment and temperature, to maintain the stability and repeatability of the FRET screening model, it is necessary to add DTT for containing Cys145 more stable and ensure the consistency of the FRET reaction conditions as much as possible [42].

Based on FRET technology, ACF and PRF with the same acridine scaffold were screened out, and showed promising inhibition of HCoV-OC43 replication in BHK-21. Their inhibition abilities are approximately same as that of Shuanghuanglian and Ebselen [9,17]. Remarkably, the IC_{50} values of ACF and PRF have reached the micron mole level, which were superior to GC376 for anti-HCoV-43, and equivalent to the standard molecule remdesivir, suggesting that they have the potential for drug repurposing. In addition, ACF has been reported to have a strong inhibitory effect on SARS-CoV-2 papain-like protease (PL^{pro}) with an IC_{50} of 1.66 μM. The antiviral activity results of ACF in cell and mouse models showed that the combination of ACF and remdesivir had a strong synergistic effect on inhibiting viral replication. Moreover, the researchers successfully resolved the co-crystal structure of ACF-PL^{pro} by X-ray crystallography. Combined with our study, we suspect that ACF and PRF might be a dual-target inhibitor of SARS-CoV-2, including but not limited to M^{pro} and PL^{pro}, which explains why ACF shows excellent antiviral activity [43]. Generally, M^{pro} and PL^{pro} are two proteases that function in the replication and packaging of new generation viruses and can handle the translation of peptides from genomic RNA to structural or non-structural proteins during viral replication. Similarly, Disulfiram and Ebselen [44–46], undergoing clinical trials, also inhibited the hydrolysis of these two proteolytic enzymes, which suggests that ACF is worthy of further study.

By confirming the enzyme kinetics, it was determined that both ACF and PRF were non-competitive inhibitors. And MST assay demonstrated that they both have a certain affinity with SARS-CoV-2 M^{pro}. Fortunately, with the simple scaffold, visual docking mechanism, and encouraging antiviral activity *in vitro*, ACF and PRF were elaborated as good candidates for the development of anti-coronaviral drugs.

5. Conclusion

In summary, we combined FRET technology, enzyme kinetics, MST, molecular docking, and cell-based antiviral assay, and finally ACF and PRF were found to be a new type of M^{pro} small molecule inhibitor with encouraging inhibitory activity. ACF and PRF were determined to be non-competitive inhibitors. Two compounds exhibited a concentration-dependent inhibition pattern against M^{pro}. Of note, our study opened a new avenue for exploring new uses of acridine scaffolds, and demonstrated that ACF was a dual-target candidate, which was a complementary to its target. As the epidemic is raging around the world, we proposed that ACF and PRF still have potential for the treatment of coronaviruses.

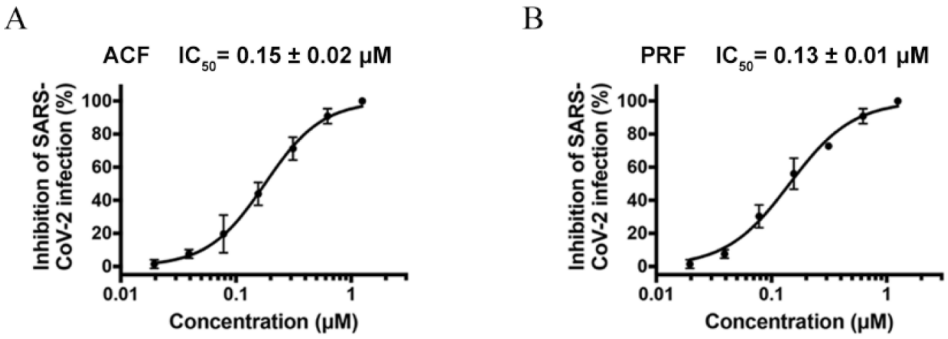

Fig. 6. Antiviral activities of the drug leads against SARS-CoV-2. Dose–response curves for ACF (A) and PRF (B) against SARS-CoV-2. All data are shown as mean ± SD, n = 3.

Declaration of Competing Interest

The authors declare that they have no known competing financial interests or personal relationships that could have appeared to influence the work reported in this paper.

Data availability

No data was used for the research described in the article.

Acknowledgments

We particularly thank Prof. Li Yan from Huazhong University of Science and Technology for grants of plasmids. Heartfelt thanks to the support and technical guidance of members in Biosafety Level 3 Laboratory of Fudan University, especially Dr. Di Qu, Xia Cai, Gaowei Hu, Qian Wang, Zhiping Sun, Yutang Li and Jing Pu.

Statements and Declarations

Funding

This work was supported by National Natural Science Foundation of China (NSFC) (No. 82141216), Chunhui Program-Cooperative Research Project of the Ministry of Education, Liaoning Province Natural Science Foundation (No. 2020-MZLH-31), Shenyang Young and Middle-aged Innovative Talents Support Program (RC210446), National Key Research and Development Program of China (2021YFC2300703) and the Shanghai Science and Technology Committee (STCSM) Science and Technology Innovation Program (No. 21S11902600).

Ethics approval

No need approval.

Competing interests

The authors declare no competing interests.

Appendix A. Supplementary material

Supplementary data to this article can be found online at https://doi.org/10.1016/j.bioorg.2022.106185.

References

[1] C. Gil, T. Ginex, I. Maestro, V. Nozal, L. Barrado-Gil, M. Cuesta-Geijo, J. Urquiza, D. Ramírez, C. Alonso, N.E. Campillo, A. Martinez, COVID-19: drug targets and potential treatments, J. Med. Chem. 63 (21) (2020) 12359–12386, https://doi.org/10.1021/acs.jmedchem.0c00606.

[2] P. V'Kovski, A. Kratzel, S. Steiner, H. Stalder, V. Thiel, Coronavirus biology and replication: implications for SARS-CoV-2, Nat. Rev. Microbiol. 19 (3) (2021) 155–170, https://doi.org/10.1038/s41579-020-00468-6.

[3] COVID-19 vaccines, Drugs and Lactation Database (LactMed), National Library of Medicine (US), Bethesda (MD), 2006.

[4] S.C. Pandey, V. Pande, D. Sati, S. Upreti, M. Samant, Vaccination strategies to combat novel corona virus SARS-CoV-2, Life Sci. 256 (2020) 117956, https://doi.org/10.1016/j.lfs.2020.117956.

[5] S.K. Saxena, S. Kumar, S. Ansari, J.T. Paweska, V.K. Maurya, A.K. Tripathi, A. S. Abdel-Moneim, Characterization of the novel SARS-CoV-2 Omicron (B.1.1.529) variant of concern and its global perspective, J. Med. Virol. 94 (4) (2022) 1738–1744, https://doi.org/10.1002/jmv.27524.

[6] B.1.1.529 (Omicron) Variant – United States, December 1–8, 2021, MMWR Morb. Mortal Wkly. Rep. 70 (50) (2021) 1731–1734, https://doi.org/10.15585/mmwr.mm7050e1.

[7] M. Xiong, H. Su, W. Zhao, H. Xie, Q. Shao, Y. Xu, What coronavirus 3C-like protease tells us: from structure, substrate selectivity, to inhibitor design, Med. Res. Rev. 41 (4) (2021) 1965–1998, https://doi.org/10.1002/med.21783.

[8] V. Anirudhan, H. Lee, H. Cheng, L. Cooper, L. Rong, Targeting SARS-CoV-2 viral proteases as a therapeutic strategy to treat COVID-19, J. Med. Virol. 93 (5) (2021) 2722–2734, https://doi.org/10.1002/jmv.26814.

[9] Z. Jin, X. Du, Y. Xu, Y. Deng, M. Liu, Y. Zhao, B. Zhang, X. Li, L. Zhang, C. Peng, Y. Duan, J. Yu, L. Wang, K. Yang, F. Liu, R. Jiang, X. Yang, T. You, X. Liu, X. Yang, F. Bai, H. Liu, X. Liu, L.W. Guddat, W. Xu, G. Xiao, C. Qin, Z. Shi, H. Jiang, Z. Rao, H. Yang, Structure of M(pro) from SARS-CoV-2 and discovery of its inhibitors, Nature 582 (7811) (2020) 289–293, https://doi.org/10.1038/s41586-020-2223-y.

[10] X.D. Xie, L.C. Hu, H. Xue, Y. Xiong, A.C. Panayi, Z. Lin, L. Chen, C.C. Yan, W. Zhou, B.B. Mi, G.H. Liu, Prognosis and treatment of complications associated with COVID-19: a systematic review and meta-analysis, Acta Mater. Med. 1 (1) (2022) 124–137, https://doi.org/10.15212/AMM-2022-0002.

[11] Z.J. Song, W.N. Nik Nabil, Z.C. Xi, H.X. Xu, Current global status and future development of traditional Chinese medicine in the prevention and treatment of coronavirus disease 2019, World J. Tradit. Chin. Med. 7 (2) (2021) 155–166, https://doi.org/10.4103/wjtcm.wjtcm_43_20.

[12] M.X. Li, Y.Y. Yang, L. Yang, M.Z. Zheng, J. Li, L.X. Chen, H. Li, Progress of traditional Chinese medicine treating COVID-19, World J. Tradit. Chin. Med. 7 (2) (2021) 167–183, https://doi.org/10.4103/wjtcm.wjtcm_68_20.

[13] S.A. Amin, T. Jha, Fight against novel coronavirus: a perspective of medicinal chemists, Eur. J. Med. Chem. 201 (2020) 112559, https://doi.org/10.1016/j.ejmech.2020.112559.

[14] R. Wang, Q. Hu, H. Wang, G. Zhu, M. Wang, Q. Zhang, Y. Zhao, C. Li, Y. Zhang, G. Ge, H. Chen, L. Chen, Identification of Vitamin K3 and its analogues as covalent inhibitors of SARS-CoV-2 $3CL^{pro}$, Int. J. Boil. Macromol. 183 (2021) 182–192, https://doi.org/10.1016/j.ijbiomac.2021.04.129.

[15] Y. Xiong, G.H. Zhu, Y.N. Zhang, Q. Hu, H.N. Wang, H.N. Yu, X.Y. Qin, X.Q. Guan, Y.W. Xiang, H. Tang, G.B. Ge, Flavonoids in Ampelopsis grossedentata as covalent inhibitors of SARS-CoV-2 $3CL^{pro}$: inhibition potentials, covalent binding sites and inhibitory mechanisms, Int. J. Boil. Macromol. 187 (2021) 976–987, https://doi.org/10.1016/j.ijbiomac.2021.07.167.

[16] C.V. Haritha, K. Sharun, B. Jose, Ebselen, a new candidate therapeutic against SARS-CoV-2, Int. J. Surg. 84 (2020) 53–56, https://doi.org/10.1016/j.ijsu.2020.10.018.

[17] H.X. Su, S. Yao, W.F. Zhao, M.J. Li, J. Liu, W.J. Shang, H. Xie, C.Q. Ke, H.C. Hu, M. N. Gao, K.Q. Yu, H. Liu, J.S. Shen, W. Tang, L.K. Zhang, G.F. Xiao, L. Ni, D. W. Wang, J.P. Zuo, H.L. Jiang, F. Bai, Y. Wu, Y. Ye, Y.C. Xu, Anti-SARS-CoV-2 activities in vitro of Shuanghuanglian preparations and bioactive ingredients, Acta Pharmacol. Sin. 41 (9) (2020) 1167–1177, https://doi.org/10.1038/s41401-020-0483-6.

[18] K. Zandi, K. Musall, A. Oo, D. Cao, B. Liang, P. Hassandarvish, S. Lan, R.L. Slack, K. A. Kirby, L. Bassit, F. Amblard, B. Kim, S. AbuBakar, S.G. Sarafianos, R.F. Schinazi, Baicalein and baicalin inhibit SARS-CoV-2 RNA-dependent-RNA polymerase, Microorganisms. 9 (5) (2021) 893, https://doi.org/10.3390/microorganisms9050893.

[19] Y. Li, S. Yu, Y. Li, X. Liang, M. Su, R. Li, Medical significance of uterine corpus endometrial carcinoma patients infected with SARS-CoV-2 and pharmacological characteristics of plumbagin, Front Endocrinol. (Lausanne) 12 (2021) 714909, https://doi.org/10.3389/fendo.2021.714909.

[20] Z. Chen, Q. Cui, L. Cooper, P. Zhang, H. Lee, Z. Chen, Y. Wang, X. Liu, L. Rong, R. Du, Ginkgolic acid and anacardic acid are specific covalent inhibitors of SARS-CoV-2 cysteine proteases, Cell Biosci. 11 (1) (2021) 45, https://doi.org/10.1186/s13578-021-00564-x.

[21] Y. Xiong, G.H. Zhu, H.N. Wang, Q. Hu, L.L. Chen, X.Q. Guan, H.L. Li, H.Z. Chen, H. Tang, G.B. Ge, Discovery of naturally occurring inhibitors against SARS-CoV-2 3CL(pro) from Ginkgo biloba leaves via large-scale screening, Fitoterapia. 152 (2021) 104909, https://doi.org/10.1016/j.fitote.2021.104909.

[22] M. Chauhan, V.K. Bhardwaj, A. Kumar, V. Kumar, P. Kumar, M.G. Enayathullah, J. Thomas, J. George, B.K. Kumar, R. Purohit, A. Kumar, S. Kumar, Theaflavin 3-gallate inhibits the main protease (M^{pro}) of SARS-CoV-2 and reduces its count in vitro, Sci. Rep. 12 (1) (2022) 13146, https://doi.org/10.1038/s41598-022-17558-5.

[23] V.K. Bhardwaj, R. Singh, J. Sharma, V. Rajendran, R. Purohit, S. Kumar, Identification of bioactive molecules from tea plant as SARS-CoV-2 main protease inhibitors, J. Biomol. Struct. Dyn. 39 (10) (2021) 3449–3458, https://doi.org/10.1080/07391102.2020.1766572.

[24] V.K. Bhardwaj, R. Singh, P. Das, R. Purohit, Evaluation of acridinedione analogs as potential SARS-CoV-2 main protease inhibitors and their comparison with repurposed anti-viral drugs, Comput. Biol. Med. 128 (2021) 104117, https://doi.org/10.1016/j.compbiomed.2020.104117.

[25] W. Vuong, M.B. Khan, C. Fischer, E. Arutyunova, T. Lamer, J. Shields, H.A. Saffran, R.T. McKay, M.J. van Belkum, M.A. Joyce, H.S. Young, D.L. Tyrrell, J.C. Vederas, M.J. Lemieux, Feline coronavirus drug inhibits the main protease of SARS-CoV-2 and blocks virus replication, Nat. Commun. 11 (1) (2020) 4282, https://doi.org/10.1038/s41467-020-18096-2.

[26] G. Jiménez-Avalos, A.P. Vargas-Ruiz, N.E. Delgado-Pease, G.E. Olivos-Ramirez, P. Sheen, M. Fernández-Díaz, M. Quiliano, M. Zimic, COVID-19 Working Group in Perú, Comprehensive virtual screening of 4.8 k flavonoids reveals novel insights into allosteric inhibition of SARS-CoV-2 M^{PRO}, Sci. Rep. 11 (1) (2021) 15452, https://doi.org/10.1038/s41598-021-94951-6.

[27] Y. Chen, X. Wang, H. Shi, P. Zou, Montelukast inhibits HCoV-OC43 infection as a viral inactivato, Viruses 14 (5) (2022) 861, https://doi.org/10.3390/v14050861.

[28] X. Wang, Y. Chen, H. Shi, P. Zou, Erythromycin estolate is a potent inhibitor against HCoV-OC43 by directly inactivating the virus particle, frontiers in cellular and infection, Microbiology (2022) 930, https://doi.org/10.3389/fcimb.2022.905248.

[29] Z. Liu, W. Xu, Z. Chen, W. Fu, W. Zhan, Y. Gao, J. Zhou, Y. Zhou, J. Wu, Q. Wang, X. Zhang, An ultrapotent pan-β-coronavirus lineage B (β-CoV-B) neutralizing antibody locks the receptor-binding domain in closed conformation by targeting its conserved epitope, Protein & cell. 13 (9) (2022) 655–675, https://doi.org/10.1007/s13238-021-00871-6.

[30] T.S. Komatsu, N. Okimoto, Y.M. Koyama, Y. Hirano, G. Morimoto, Y. Ohno, M. Taiji, Drug binding dynamics of the dimeric SARS-CoV-2 main protease, determined by molecular dynamics simulation, Sci. Rep. 10 (1) (2020) 16986, https://doi.org/10.1038/s41598-020-74099-5.

[31] L. Zhang, D. Lin, Y. Kusov, Y. Nian, Q. Ma, J. Wang, A. von Brunn, P. Leyssen, K. Lanko, J. Neyts, A. de Wilde, E.J. Snijder, H. Liu, R. Hilgenfeld, α-Ketoamides as broad-spectrum inhibitors of coronavirus and enterovirus replication: structure-based design, synthesis, and activity assessment, J. Med. Chem. 63 (9) (2020) 4562–4578, https://doi.org/10.1021/acs.jmedchem.9b01828.

[32] J.W. Zhang, Y. Xiong, F. Wang, F.M. Zhang, X. Yang, G.Q. Lin, P. Tian, G. Ge, D. Gao, Discovery of 9,10-dihydrophenanthrene derivatives as SARS-CoV-2 $3CL^{pro}$ inhibitors for treating COVID-19, Eur. J. Med. Chem. 228 (2022) 114030, https://doi.org/10.1016/j.ejmech.2021.114030.

[33] L. Shen, J. Niu, C. Wang, B. Huang, W. Wang, N. Zhu, Y. Deng, H. Wang, F. Ye, S. Cen, W. Tan, High-throughput screening and identification of potent broad-spectrum inhibitors of coronaviruses, J. Virol. 93 (12) (2019) e00023–e00119, https://doi.org/10.1128/JVI.00023-19.

[34] W.T. Harvey, A.M. Carabelli, B. Jackson, R.K. Gupta, E.C. Thomson, E.M. Harrison, C. Ludden, R. Reeve, A. Rambaut, S.J. Peacock, D.L. Robertson, SARS-CoV-2 variants, spike mutations and immune escape, Nat. Rev. Microbiol. 19 (7) (2021) 409–424, https://doi.org/10.1038/s41579-021-00573-0.

[35] R. Banerjee, L. Perera, L.M.V. Tillekeratne, Potential SARS-CoV-2 main protease inhibitors, Drug Disc. Today. 26 (3) (2021) 804–816, https://doi.org/10.1016/j.drudis.2020.12.005.

[36] W.C. Chiou, M.S. Hsu, Y.T. Chen, J.M. Yang, Y.G. Tsay, H.C. Huang, C. Huang, Repurposing existing drugs: identification of SARS-CoV-2 3C-like protease inhibitors, J. Enzyme Inhib. Med. Chem. 36 (1) (2021) 147–153, https://doi.org/10.1080/14756366.2020.1850710.

[37] M. Lu, P.D. Uchil, W. Li, D. Zheng, D.S. Terry, J. Gorman, W. Shi, B. Zhang, T. Zhou, S. Ding, R. Gasser, J. Prévost, G. Beaudoin-Bussières, S.P. Anand, A. Laumaea, J.R. Grover, L. Liu, D.D. Ho, J.R. Mascola, A. Finzi, P.D. Kwong, S. C. Blanchard, W. Mothes, Real-time conformational dynamics of SARS-CoV-2 spikes on virus particles, Cell Host Microbe. 28 (6) (2020) 880–891.e8, https://doi.org/10.1016/j.chom.2020.11.001.

[38] K. Gorshkov, D.M. Vasquez, K. Chiem, C. Ye, B.N. Tran, J.C. de la Torre, T. Moran, C.Z. Chen, L. Martinez-Sobrido, W. Zheng, A SARS-CoV-2 nucleocapsid protein TR-FRET assay amenable to high-throughput screening, ACS Pharmacol. Transl. Sci. 5 (1) (2022) 8–19, https://doi.org/10.1101/2021.07.03.450938.

[39] D.A. Jans, K.M. Wagstaff, The broad spectrum host-directed agent ivermectin as an antiviral for SARS-CoV-2, Biochem. Biophys. Res. Commun. 538 (2021) 163–172, https://doi.org/10.1016/j.bbrc.2020.10.042.

[40] H. Kared, A.D. Redd, E.M. Bloch, T.S. Bonny, H. Sumatoh, F. Kairi, D. Carbajo, B. Abel, E.W. Newell, M.P. Bettinotti, S.E. Benner, E.U. Patel, K. Littlefield, O. Laeyendecker, S. Shoham, D. Sullivan, A. Casadevall, A. Pekosz, A. Nardin, M. Fehlings, A.A. Tobian, T.C. Quinn, SARS-CoV-2-specific CD8+ T cell responses in convalescent COVID-19 individuals, J. Clin. Invest. 131 (5) (2021) e145476, https://doi.org/10.1172/jci145476.

[41] C.P. Chuck, C. Chen, Z. Ke, D.C. Wan, H.F. Chow, K.B. Wong, Design, synthesis and crystallographic analysis of nitrile-based broad-spectrum peptidomimetic inhibitors for coronavirus 3C-like proteases, Eur. J. Med. Chem. 59 (2013) 1–6, https://doi.org/10.1016/j.ejmech.2012.10.053.

[42] C. Ma, Y. Hu, J.A. Townsend, P.I. Lagarias, M.T. Marty, A. Kolocouris, J. Wang, Ebselen, disulfiram, carmofur, PX-12, tideglusib, and shikonin are non-specific promiscuous SARS-CoV-2 main protease inhibitors, ACS Pharmacol. Transl. Sci. 3 (6) (2020) 1265–1277, https://doi.org/10.1101/2020.09.15.299164.

[43] V. Napolitano, A. Dabrowska, K. Schorpp, A. Mourão, E. Barreto-Duran, M. Benedyk, P. Botwina, S. Brandner, M. Bostock, Y. Chykunova, A. Czarna, G. Dubin, T. Fröhlich, M. Hölscher, M. Jedrysik, A. Matsuda, K. Owczarek, M. Pachota, O. Plettenburg, J. Potempa, I. Rothenaigner, F. Schlauderer, K. Slysz, A. Szczepanski, K. Greve-Isdahl Mohn, B. Blomberg, M. Sattler, K. Hadian, G. M. Popowicz, K. Pyrc, Acriflavine, a clinically approved drug, inhibits SARS-CoV-2 and other betacoronaviruses, Cell Chem. Biol. 29 (5) (2022) 774–784.e8, https://doi.org/10.1016/j.chembiol.2021.11.006.

[44] C. Ma, H. Tan, J. Choza, Y. Wang, J. Wang, Validation and invalidation of SARS-CoV-2 main protease inhibitors using the Flip-GFP and Protease-Glo luciferase assays, Acta Pharm. Sin. B. 12 (4) (2022) 1636–1651, https://doi.org/10.1016/j.apsb.2021.10.026.

[45] M.H. Lin, D.C. Moses, C.H. Hsieh, S.C. Cheng, Y.H. Chen, C.Y. Sun, C.Y. Chou, Disulfiram can inhibit MERS and SARS coronavirus papain-like proteases via different modes, Antiviral Res. 150 (2018) 155–163, https://doi.org/10.1016/j.antiviral.2017.12.015.

[46] P.A. Nogara, F.B. Omage, G.R. Bolzan, C.P. Delgado, M. Aschner, L. Orian, J. B. Teixeira Rocha, In silico Studies on the Interaction between Mpro and PLpro From SARS-CoV-2 and Ebselen, its Metabolites and Derivatives, Mol. Inform. 40 (8) (2021), https://doi.org/10.1002/minf.202100028.